APRIL-1995 CB-NOTE XXX

Technical report of the 10 photon final state and the 5 π_0 final state partial wave analysis

Stefan Resag

Institut für Strahlen– und Kernphysik, Universität Bonn, D–53115 Bonn, Germany

Chapter 1

Preselection

The data for the analysis of the 10 photon final state in liquid hydrogen were collected in eight run periods with a special 0 prong trigger. The following cuts were applied on the data in a first selection step:

1. Successfull tracking
2. No charged tracks allowed in the JDC
3. Exactly 10 photons above 20.0 MeV (EPEDBC = 20.0 MeV)
4. Energy of central crystal above 10.0 MeV to avoid split-offs.
5. Inv. shower mass of single-PED-cluster below 100.0 MeV
6. Reject PED'S with central crystal of type 13 (outer ring of barrel)
7. E-,$\vec{p}$-conservation: require 1600 MeV $\leq E_{tot} \leq$ 2100 MeV, $|\vec{P}_{tot}| \leq$ 160 MeV

Table 1.1 gives a survey of the data reduction for the zero-prong triggered data.

run period	1	2	3	4	5	6	7
Dec. '89	1195337	1121970	128737	126989	126962	92784	82338
Jun. '90	1405739	1267573	148344	145959	145923	105716	86906
Jul. '90	3591485	3226962	387555	382362	381983	286975	239695
Sept. '90	1313069	1145485	143023	138247	138069	103525	88710
Nov. '90	4568545	4140638	532309	524281	523789	396962	342969
May '91	1561846	1368681	175128	171968	171794	131052	114014
Jun. '91	846517	777683	96856	95451	95393	72317	63346
Aug. '91	1684921	1484951	172436	131837	130767	82059	71121
Sum	16167459	13833943	1784388	1717094	1714680	1271390	1089099

Table 1.1: *The result of the first selection steps.*

Chapter 2

Kinematic fitting

After preselection the remaining data were fitted kinematically. For this purpose we used the standard program CBKFIT. The main problem of analysing this channel is the huge number of combinations possible to form $5\pi^0$ (#comb. = 945) or $4\pi^0$ and one η (#comb. = 4725) out of 10 γ. Often more than one hypothesis or combination of photons yields a good confidence levels. Only the combination with the highest confidence level for each hypothesis was taken into further analysis.

The following hypotheses were fitted:

$$\begin{aligned} \bar{\mathrm{p}}\mathrm{p} &\rightarrow 10\gamma \quad (4\mathrm{C}) \\ \bar{\mathrm{p}}\mathrm{p} &\rightarrow 5\pi^0 \quad (9\mathrm{C}) \\ \bar{\mathrm{p}}\mathrm{p} &\rightarrow 4\pi^0\eta \quad (9\mathrm{C}) \end{aligned} \tag{2.1}$$

Of course, several additional hypotheses with η', 2η, or ω can be applied to the 10γ final state, but there is no evidence for any strong η' signal or any ω with one missing γ, as can be seen from the 2γ invariant mass distributions (fig. 2.1 c)).

To distinguish between the $5\pi^0$ and the $4\pi^0\eta$ hypothesis, we used the following cuts:

- successful fit of 10γ hypothesis (CL $\geq 1\%$)
- $\mathrm{Cl}(\bar{\mathrm{p}}\mathrm{p}\rightarrow 5\pi^0) \geq 10\%$ or $\mathrm{Cl}(\bar{\mathrm{p}}\mathrm{p}\rightarrow 4\pi^0\eta) \geq 10\%$
- $\frac{\mathrm{Cl}(\bar{\mathrm{p}}\mathrm{p}\rightarrow 5\pi^0)}{\mathrm{Cl}(\bar{\mathrm{p}}\mathrm{p}\rightarrow 4\pi^0\eta)} \geq \tan(75^\circ)$. This is due to a roughly estimated selection efficiency ration of 6:1 for these two channels

Additionally for the $4\pi^0\eta$ mode, it was required, that at least one, but at most two combinations fulfill the following expression:

$$\sqrt{\sum_{i=1,4}^{4} (m(\gamma_{i1}\gamma_{i2}) - m_{\pi^0})^2 + (m(\gamma_{j1}\gamma_{j2}) - m_\eta)^2)/4} \quad \leq \quad 25\mathrm{MeV} \tag{2.2}$$

Here $m(\gamma_{i1}\gamma_{i2})$ means the invariant mass of a particle, which has as 4-momentum the sum of the two photon 4-momenta. The factor 1/4 on the left side of the equation was adjusted with Monte Carlo events and is due to the larger experimental errors at higher energies and momenta. We allow two combinations, to take two exchanged soft photons

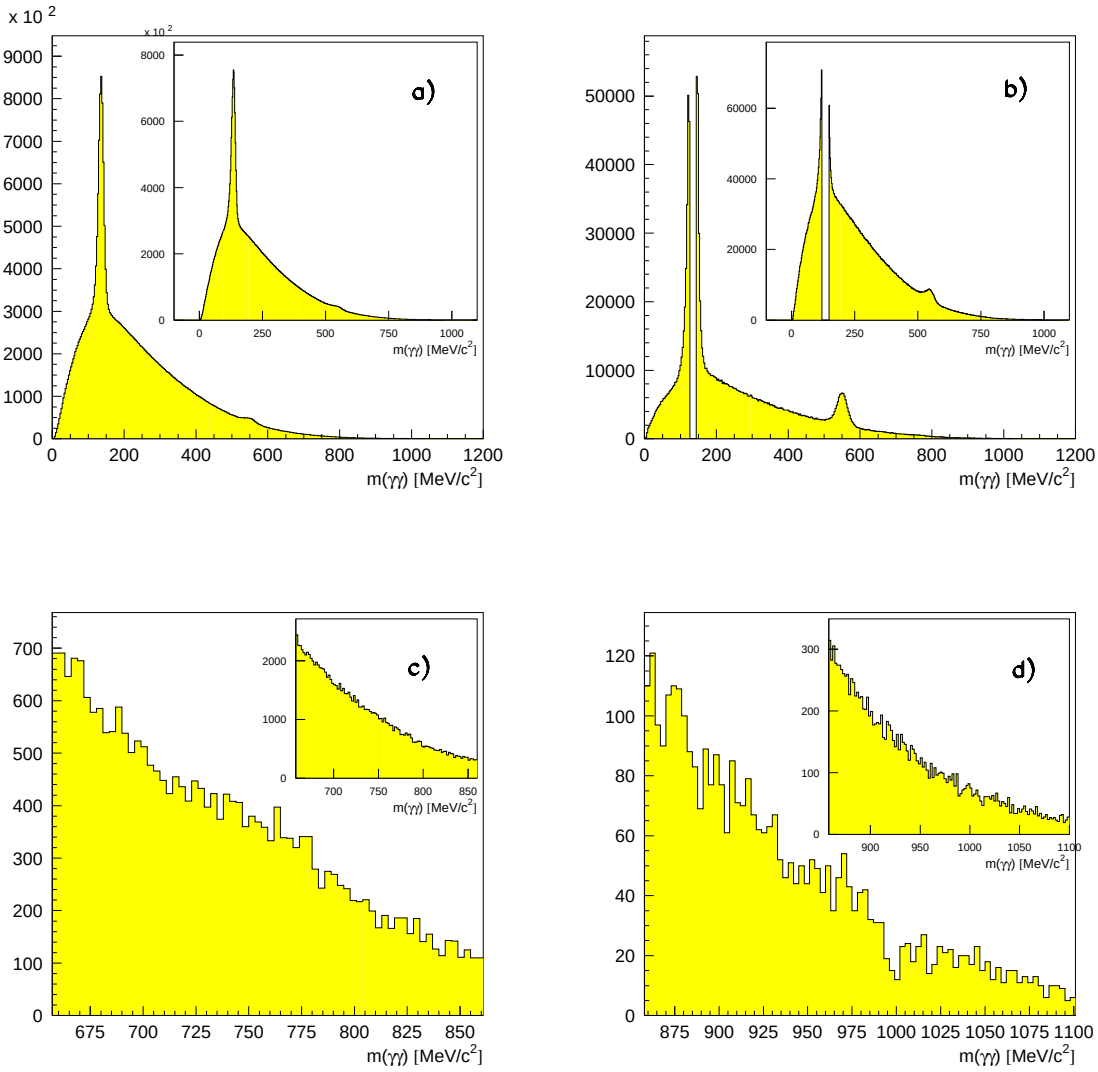

Figure 2.1: *$\gamma\gamma$ invariant mass distribution. Large pictures: kinematically fitted data;small pictures: tracked data. a): all $\gamma\gamma$ combinations, b): reject combinations with photons, which form a π^0,c) and d): reject combinations with photons, forming a π^0 or an η. c): ω-region, d): η'-region.*

run period	4C-fit	$5\pi^0$	$4\pi^0\eta$
Dec. '89	59159	30195	4833
Jun. '90	65014	33396	5368
Jul. '90	170516	88475	14536
Sept. '90	64506	33297	5582
Nov. '90	239193	120438	19037
May '91	82315	43433	6943
Jun. '91	42773	20791	3309
Aug. '91	50298	25337	4064
Sum	773774	396362	63899

Table 2.1: *Result of the kinematic fit, the $5\pi^0$ values are given after subtraction of the $\eta\pi\pi$ events.*

into account. This additional cut (AC) can also be applied to the $5\pi^0$ final state, but the reduction of background is too small in comparison to loss of acceptance (see tab. 2.2).

The results of the kinematic fit together with the additional cuts are given in table 2.1.

The combinatorical background and background from other final states was estimated via Monte Carlo events, produced with CBGEANT. We respectivly analysed 50000 $5\pi^0$ and $4\pi^0\eta$ Monte Carlo events with the whole analysis chain and in addition with the cut discribed in eq. 2.2. Then we investigated the number of events, which were put back together in the right way. The results can be found in table 2.2. In the left column $5\pi^0$ AC means, we analysed $5\pi^0$ Monte Carlo data using the additional cut in the selection chain for both final states. The other columns show the number of events found at all and give the background contribution due to wrong combinations or hypotheses. The $5\pi^0$ numbers were multiplied with a factor of 4.5 to take into account the larger branching ratio of this channel.

For the $4\pi^0\eta$ final state, the additional cut leads to a significiant reduction of combinatorical and $5\pi^0$ background. Notice, that we aim for 5 correctly reconstructed particles. In most cases at least three of the five final particles were put together in the right way, so that the effective background is somewhat smaller than tab. 2.2 implies.

	$5\pi^0$	right	wrong	$4\pi^0\eta$	right	wrong
$5\pi^0$ AC	23976	22189	1773	491	0	491
$5\pi^0$	27693	24804	2889	599	0	599
$4\pi^0\eta$ AC	250	0	250	4431	4044	387
$4\pi^0\eta$	314	0	314	5387	4647	740

Table 2.2: *Background estimates*

To achieve flat confidence level distributions and gaussian shaped pulls several error scalings were tried for different run periods. In table 2.3 the scaling factors which were used are listed.

run period	energy	θ	ϕ
Nov '90	0.029	1.4	1.4
all other run-periods	0.032	1.5	1.5
Monte Carlo	0.030	1.5	1.5

Table 2.3: *Correction factors for the kinematic fit*

Notice that for run period November '90 the error scaling factors are significiantly smaller in comparison to all other run periods, which may be due to a better callibration of the data. Also the confidence levels for this run period were found to be more flat.

The confidence level distributions for the different hypotheses are shown in fig 2.2. Especially for the hypothesis $4\pi^0\eta$, the cuts used for separation of the two channels lead to a much flatter distribution which means a good reduction of background. Nevertheless a reasonable amount of background has to be taken into acount in the $4\pi^0\eta$ final state. In figure 2.2 d), the confidence levels for both hypotheses are plotted against each other. Note the logarithmic scale on the z-axis.

Figure 2.3 shows the pulls for the three kinematic quantities. The gaussian function describes the distribution rather well with a standard deviation of ≈ 1 and a mean value of ≈ 0 except for $\sqrt{E}$. The exact values are given in table 2.4. For the θ-pulls, a variation in the z-position of the vertex could be due to the somewhat worse fit values. For the energy pulls, only part of the distribution is fitted with a gaussian.

	$\bar{x}_\phi$	σ_ϕ	$\bar{x}_\theta$	σ_θ	$\bar{x}_{\sqrt{E}}$	$\sigma_{\sqrt{E}}$
10 γ	-0.310^{-3}	1.002	-0.13	1.08	0.19	0.983

Table 2.4: *Mean and standard deviation of the pulls.*

The acceptance of the detector can be checked with the decay angular distributions in the process $\pi^0 \to \gamma\gamma$ and $\eta \to \gamma\gamma$ (see fig 2.4). Here θ is the angle between pion and photon momentum in the restframe of the pion. The distributions are almoust flat (see fig. 2.4). The loss of acceptance for decays with very small θ is due to the fact, that one photon needs a minimum energy of 20 MeV to be detected.

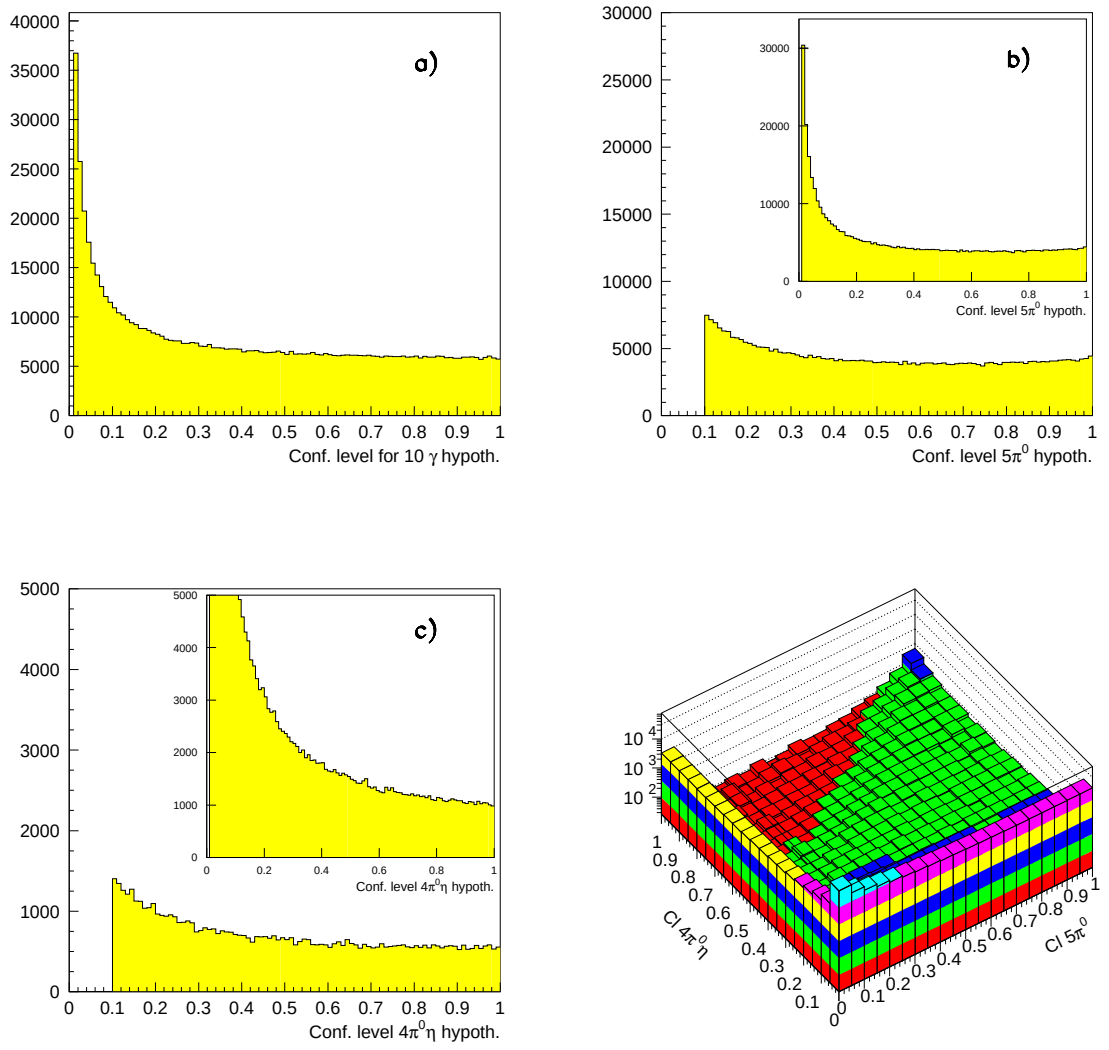

Figure 2.2: *Confidence level distributions. Small pictures: distributions found by CBKFIT without additional seperation between $5\pi^0$ and $4\pi^0\eta$. Large pictures: distributions with all cuts.*

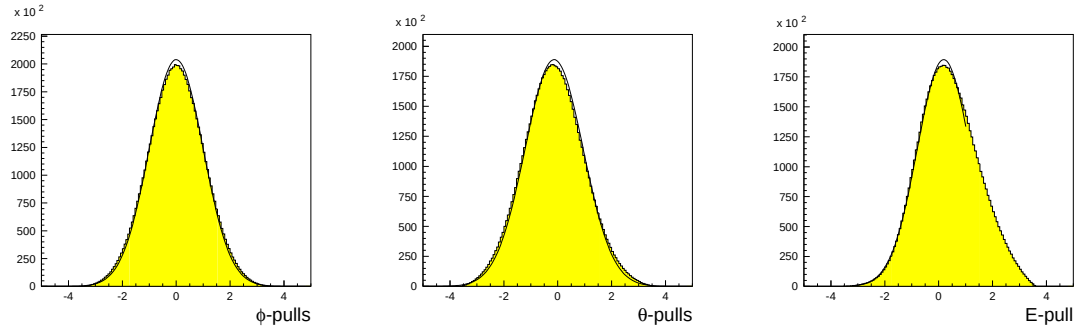

Figure 2.3: *Distribution of the pulls for the three kinematic quantities θ, ϕ and $\sqrt{E}$ for 4C-fit.*

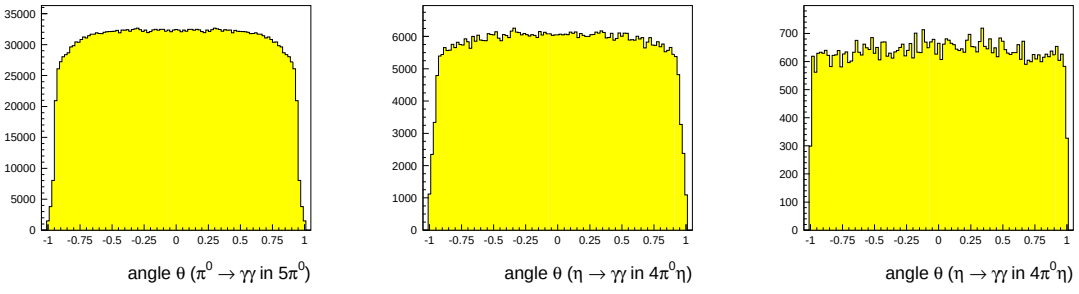

Figure 2.4: *Distribution of angle θ in $5\pi^0/\eta \to \gamma\gamma$ decays.*

Chapter 3

The $4\pi^0\eta$ final state

The main emphasis of the present analysis is the $5\pi^0$ final state. Nevertheless in this chapter we want to present the invariant mass spectra and the $\eta'\pi^0\pi^0$ and $\eta\eta\pi^0$ Dalitz plots for the $4\pi^0\eta$ final state. In fig. 3.1 the possible invariant mass distributions are shown. We see a very clear η signal in the $3\pi^0$ inv. mass distribution above a quite small background. All events with a $3\pi^0$ inv. mass lying between 523 MeV and 561 MeV were again fitted using the hypothesis $\bar{p}p \to \eta\eta\pi^0$ ($\eta \to 3\pi^0$). This leads to a sample of 17513 $\eta\eta\pi^0$ events.

In the $\eta\pi^0\pi^0$ inv. mass distributions besides a very large η' signal a clear shoulder at about 1400 MeV is observed. A possible explanation could be the $\eta\pi^0\pi^0$ decay mode of the E-Meson.

After subtraction of the $\eta\eta\pi^0$ and $\eta'\pi^0\pi^0$ background the $2\pi^0$, $4\pi^0$ and $3\pi^0\eta$ show no clear signal even though there is a very steep rise of intensity in the $4\pi^0$ inv. mass distribution near the upper phase space limit. In the $\pi^0\eta$ inv. mass distribution a clear $a_0(980)$ signal is seen.

In figure 3.3 we show the $\eta\eta\pi^0$ Dalitz plot (#events = 17513). It clearly shows the same features as the Dalitz plot in the 6γ final state: Two crossing bands due to the $a_0(980)$ and two diagonal structures in the $\eta\eta$ channel at about 1500 MeV and 1370 MeV.

At next we tried a fit to the data within the K-matrix formalism also used in the analysis of the $\eta\eta\pi^0$ final state in the 6 photon channel [1] [2]. For the $\pi\eta$ S-wave we fixed the pole positions to the values found in [3],i.e., introducing two 2×2 K-matrix poles corresponding to the $a_0(980)$ and $a_0(1450)$ as obtained in [3] and let the production strengths and phases free. The $\pi\pi$ S-wave was introduced as a 1×1 K-matrix with three variable poles. For the only possible 2^{++} $\pi\eta$ resonance, the $a_0(1320)$, we used fixed mass and width taken from [4] and again leave the production strength and phase free. The 2^{++} $\eta\eta$ S-wave is described using a single pole with all parameters free.

This hypothesis was applied to the $\pi\eta\eta$ Dalitz plot. The fit found a χ^2 of 1909 for 1687 fitted Dalitz plot cells, which means:

$$\chi^2_{ndf} = 1.16 \text{ (in } 10\gamma \text{ channel)} \quad (3.1)$$

$$\chi^2_{ndf} = 1.23 \text{ (in } 6\gamma \text{ channel)} \quad (3.2)$$

which is even better than in the 6 photon analysis due to the much lower statistics used in the 10 photon analysis. In fig. 3.2, several mass distributions and decay angular distributions are compared for data and fit. In table 3.1 the production strengths and phases for the fixed poles are shown. Table 3.2 gives the T-matrix poles and production

strengths for the variable resonances. The values for the 6γ hypothesis are taken from hypothesis no. 9 of [1]. We have a good all over agreement of the fit-parameter for the 6- and the 10-photon final state. Note that we have used a Dalitz plot without acceptance correction. This could require the worse values for the AX-meson ($I(J^{PC}) = 0(2^{++})$).

		6γ		10γ	
$I^G(J^{PC})$	particle	$\|\beta\|$	$arg(\beta)$	$\|\beta\|$	$arg(\beta)$
$1^-(0^{++})$	$a_0(980)$	0.14	-	0.17	-
	$a_0(1450)$	0.79	2.09	0.87	1.69
$1^-(2^{++})$	$a_2(1320)$	0.14	2.07	0.12	2.17

Table 3.1: *Production strengths for fixed resonances.*

Of course this partial wave analysis is very crude but at least it shows, that we have a good understanding of the acceptance of the detector and that we are able to handle a many photon final state. The advantage of the $\eta\eta\pi^0$ channel lies in a further reduction of $5\pi^0$ background due to the additional cut in the $3\pi^0$ inv. mass distribution, combined with a kinematic fit using the $\eta\eta\pi^0$ hypothesis.

	6γ			
$I^G(J^{PC})$	mass (MeV)	width (MeV)	$\|\beta\|$	$arg(\beta)$
$0^+(0^{++})$	1393	288	0.16	-4.10
	1499	136	0.29	8.5
	$130 \cdot 10^3$	21	1017	7.04
$0^+(2^{++})$	1547	113	0.15	15.77
	10γ			
$I^G(J^{PC})$	mass (MeV)	width (MeV)	$\|\beta\|$	$arg(\beta)$
$0^+(0^{++})$	1431	168	0.11	-3.76
	1525	126	0.20	8.83
	$131 \cdot 10^3$	28	980	6.96
$0^+(2^{++})$	1563	248	0.16	17.08

Table 3.2: *T-matrix poles and production strengths for the variable resonances.*

To create a $\eta'\pi^0\pi^0$ Dalitz plot, we have to reduce the background, which is about 30% of the size of the signal. Since the background below the η' signal is almost linear, we try a sideband subtraction. This is done in the following steps:

- select events lying in one of the three mass windows: (927 MeV - 939 MeV),(945 MeV 969 MeV),(975 MeV - 987 MeV). For a linear background, the numer of background events in the right plus left window and the middle window are identical
- multiply energy and momentum of particles with a factor of 957.75 MeV/m($\eta\pi^0\pi^0$) to adjust the inv. mass to the η' mass
- fit events using the hypothesis $\eta'\pi^0\pi^0$
- subtract Dalitz plots for side bins from the Dalitz plot of middle bins

This leads to 13006 events without background subtraction and effectivly 8816 events after subtraction of background. The plots without and with sidebin subtraction are shown in fig. 3.3. After reduction of background, the enhancement at the edge of the Dalitz plot vanishes. We notice a band like structure at an $\eta'\pi^0$ inv. mass of about 1320 MeV, which may be due to an $a_2(1320)$. The structure in the center could be an interference of resonances in the $\eta'\pi^0$ channel and the $\pi\pi$ s-wave. Here a partial wave analysis is needed.

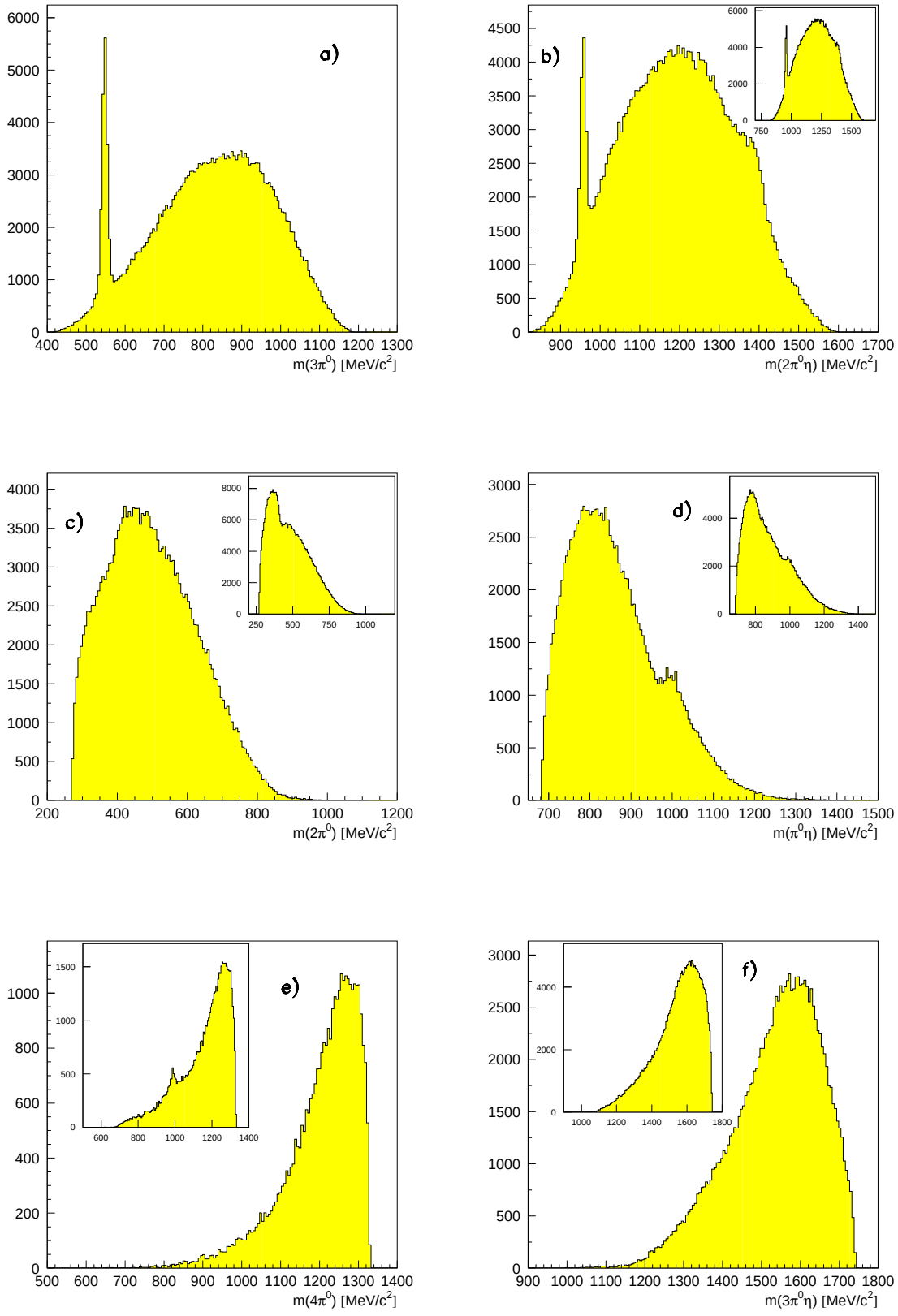

Figure 3.1: *Invariant mass distributions of the $4\pi^0\eta$ final state. Small pictures: without subtraction of the $\eta\eta\pi^0$ and $\eta'\pi^0\pi^0$ final state. Large pictures: subtraction, where possible*

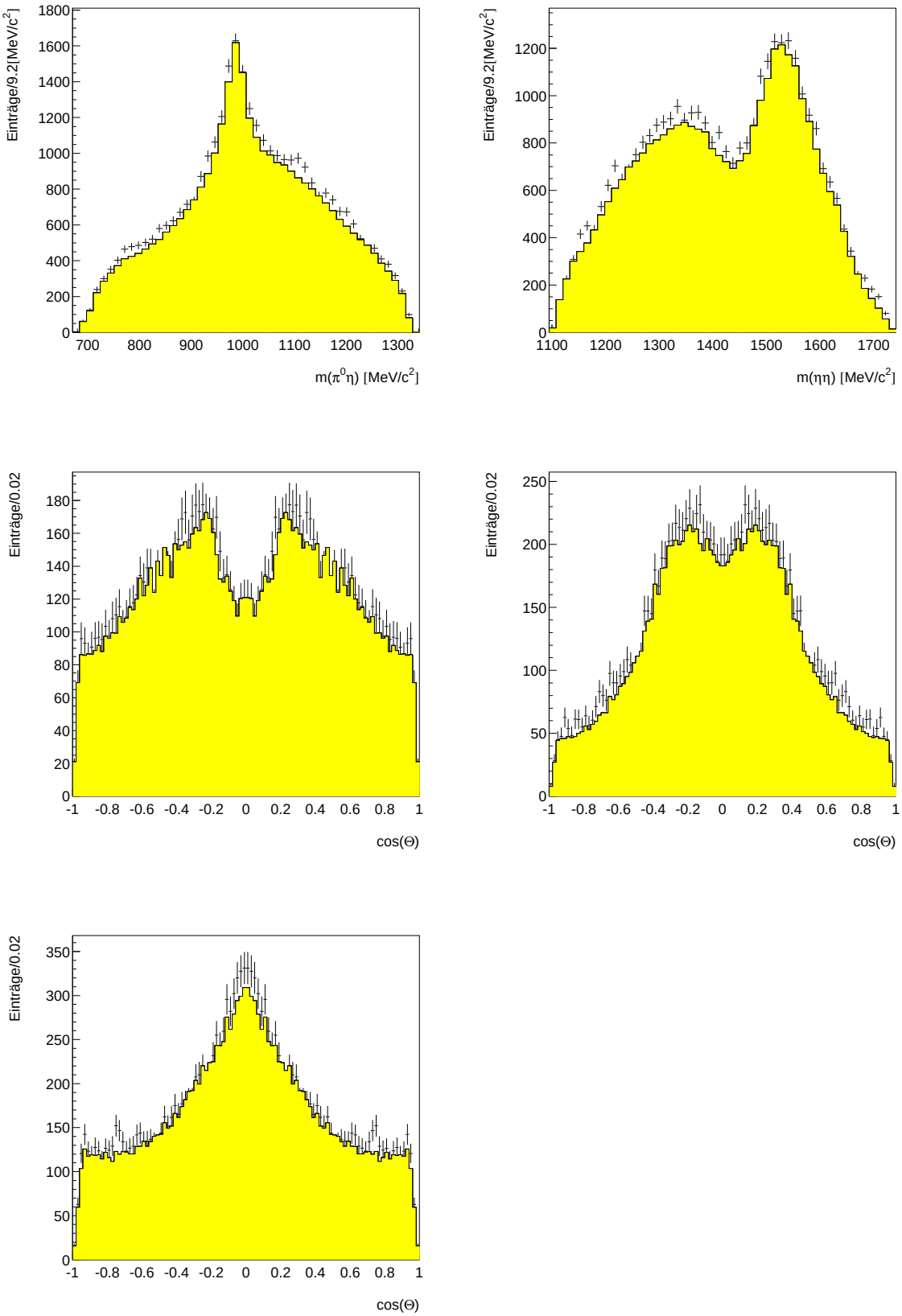

Figure 3.2: *Fitresult:* $\pi^0\eta$ *projection,* $\eta\eta$ *projection, angular distribution in* $\pi^0\eta$*:* $(980 \pm 30) MeV/c^2$*. Angular distribution in* $\eta\eta$*:* $(1400 \pm 50) MeV/c^2$ *and* $(1515 \pm 50) MeV/c^2$*.*

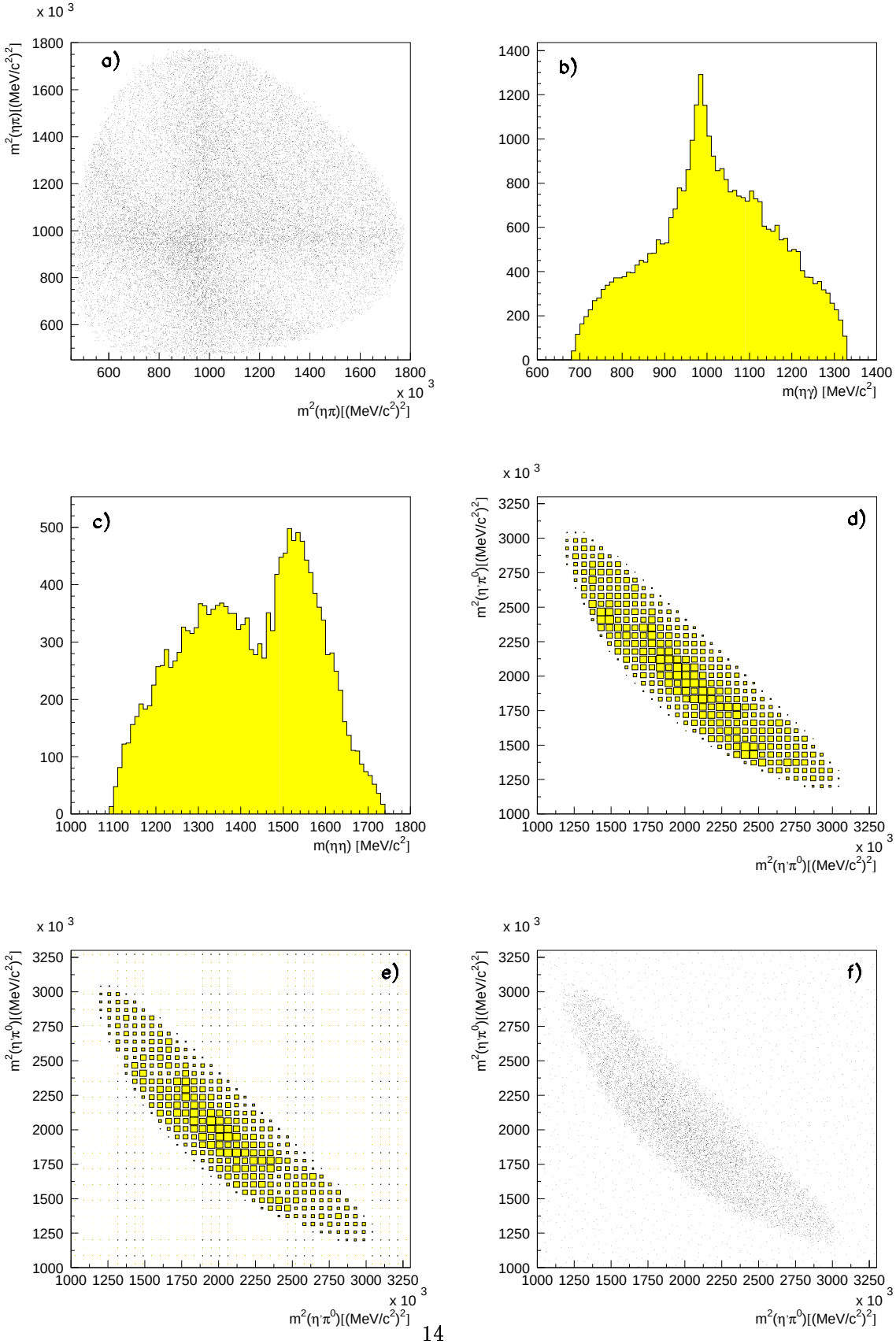

Figure 3.3: *The $\eta\eta\pi^0$ and $\eta'\pi^0\pi^0$ channel. d): $\eta'\pi^0\pi^0$ Dalitz plot without sidebin subtraction. e) & f): $\eta'\pi^0\pi^0$ Dalitz plot with sidebin subtraction.*

Chapter 4

The $5\pi^0$ final state

The main purpose of this report is to give a partial wave analysis of the $5\pi^0$ final state. First of all we have to define some suitable kinematic variables to describe an event. We start with 20 kinematic variables for a final state of five pseudoskalar mesons, which correspond to five 4-vectors. After applying the usual constraints namely energy and momentum conservation, mass shell behaviour of the π^0 or η and rotation symmetry for $\bar{p}p$ annihilation at rest, we end up with 8 independent variables. One set of variables is for example: $(m_A, m_B, m_C, \theta_{AB}, \theta_{B\pi}, \phi_{B\pi}, \theta_{C\pi}, \phi_{C\pi})$. Here m_A is the inv. mass of 4 pions, m_B and m_C are the inv. masses of the two 2-pion subsystems at a time. All angles are declared in the rest frames of the decaying particles. For explanation of these variables see also fig. 4.1.

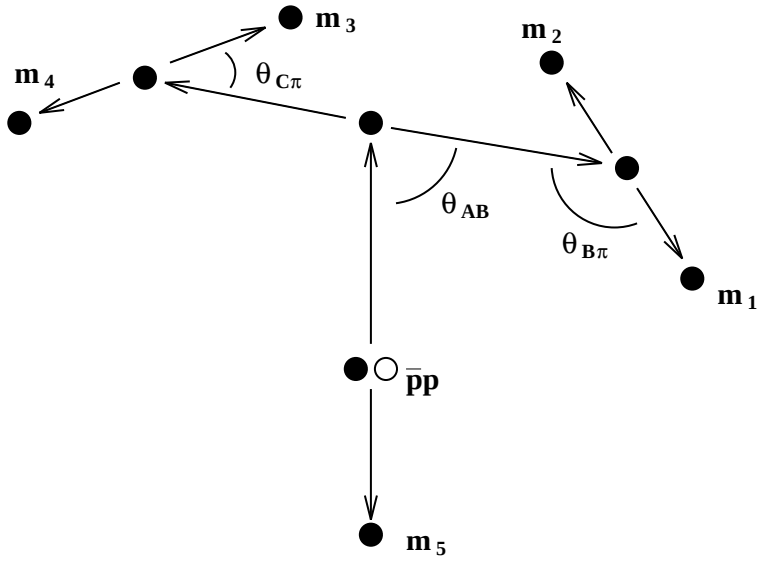

Figure 4.1: *Definition of decay angles*

In figure 4.2 we show the invariant mass and decay anglular distributions of the $5\pi^0$ final state compared to Monte Carlo events. Since we have five identical particles, the decay angular distributions for $B \to \pi^0\pi^0$ and $C \to \pi^0\pi^0$ were added. All decay angular distributions are almoust flat. This means, we don't have a loss of acceptance in some kinematical region coming from cuts in the selection chain or the geometry of the detector.

For all distributions the data show significant deviations from phase space behaviour. In the $3\pi^0$ inv. mass distribution a clear η signal is seen. Because of the smallness of phasespace in the η region, these events can be cut out easily or respectivly $\eta 2\pi^0$ events can be selected with just a small background due to combinatorics. By cutting out these events, the resonance like structure in the $2\pi^0$ inv. mass vanishes as just being a reflection of these events. Also the shape of the $4\pi^0$ inv. mass distributions changes significiantly. A resonance like structure with a mass of about 1450 MeV remains.

Next all events with a $3\pi^0$ invariant mass lying between 523 and 561 MeV were fitted using the $\eta\pi^0\pi^0$ hypothesis. In fig. 4.3 we show the $\pi\pi\eta$ Dalitz plot together with the $\pi\eta$ inv. mass distributions.

For completion we show the $3\pi^0$ Dalitz plot from the decay $\eta \rightarrow 3\pi^0$ and the corresponding radial density (see fig 4.3).

4.1 Likelihood fit

Since one event of the $5\pi^0$ final state is described via 8 kinematic variables it is not possible to apply any binned fit to the data. Asuming a binning of 5 per variable, we have on an average 1 event per bin and most bins are edge bins. Also it is not sufficient to do a χ^2 fit for a set of Dalitz plots or projections without loss of information. The whole information is only available in an unbinned Likelihood fit. In the following we give a short introduction to the method of likelihood fitting.

Let $w(\vec{x},\vec{p})$ be the probability distribution of the variable $\vec{x} \in X$. We let this distribution also depend on a set of parameters $\vec{p}$. In our case X is equal to the attainable kinematic region of the process and $\vec{p}$ is a set of fit parameters like masses and widths. Since w is a probability distribution, it has to be normalized for every set of parameters $\vec{p}$:

$$\int w_(\vec{x},\vec{p})d\vec{x} \quad = 1 \tag{4.1}$$

were the integral is calculated over the whole phase space. Then $w(\vec{x}_i,\vec{p})$ describes the production probability of an event having the measured kinematic properties $\vec{x}_i$.

The Likelihood funktion is defined in eq. 4.2.

$$\mathcal{L}_{\vec{\checkmark}} \quad = \quad \prod_{i=1}^{N} w(\vec{x}_i,\vec{p}) \tag{4.2}$$

It is just the product of the propabilities of N measured events. This function now has to be maximized by varying the parameters $\vec{p}$, to get the best agreement between theoretical hypothesis and experiment. To achieve automatically normalized weights, we make the following substitution:

$$w \quad \rightarrow \quad \frac{w}{\int_X w dx} \tag{4.3}$$

In general the fitting is done by minimizing the negative logarithm of eq. 4.2 or eq. 4.3.

$$-ln(\mathcal{L}) \quad = \quad N ln\left(\int w dx\right) - \sum_{i=1}^{N} w_i \tag{4.4}$$

The normalization integral usually is calculated with Monte Carlo events:

$$\int w dx \quad \rightarrow \quad \sum_{j}^{M} w(\vec{x}_j) \tag{4.5}$$

Now let us look more closely at the weights w_i. We can express these as $w_i = \xi_i \cdot \phi_i \cdot \epsilon_i$, were ϵ is the detection efficiency, ϕ is the phace space weight and ξ is some dynamical weight of the event. Inserting this in eq. 4.6 we get:

$$-ln(\mathcal{L}) \quad = \quad Nln(\sum^{M} w) - \sum^{N} ln\xi_1 - \sum^{N} ln(\phi_i \epsilon_i) \tag{4.6}$$

If we always use the same set of events for fitting, the last sum of eq. 4.6 is a constant and can be neglected when minimizing $-ln(\mathcal{L})$. Let us now have a look on the normalization integral. As mentioned above it often is calculated using M Monte Carlo events. In our analysis we used events produced according to phase space, so ϕ is equal to 1. The detection efficiency is 1, if the event passes through the analysis chain, else it is zero. Eq. 4.6 reduces to

$$-ln(\mathcal{L}) \quad = \quad Nln(\sum_{i=1}^{M} \xi_i \epsilon_i) - \sum_{i=1}^{N} ln\xi_i. \tag{4.7}$$

4.2 $5\pi^0$ partial wave analysis

The partial wave analysis of the $5\pi^0$ final state is carried out using the K-matrix formalism [5]. In order to figure out the dominant contributions to that final state a huge number of fits were made. We only take annihilation from the ${}^1S_0$-initial state into account. The analysis was done using the isobar model. In contrast to the analysis of final states with three pseudoscalar mesons, we not just have two-meson-, but also three- and four-meson-interaction. For the three-meson interaction, we only try the $\pi_0(1300)$, recoiling against a $\pi\pi$ S-wave. The decay of the $\pi_0(1300)$ is described by a second $\pi\pi$ S-wave, so that the production vector becomes

$$F \quad = \quad BW_{\pi(1300)} \cdot \hat{T}_{11} \cdot \hat{T}_{11} \tag{4.8}$$

For the $\pi\pi$ S-wave we use a 2×2 K-matrix. The corresponding T-matrix poles are listed in table 4.1. They were taken from the partial wave analysis of the $3\pi^0$ final state [6].

Pol	m $[MeV/c^2]$	$\tilde{\Gamma}_{\pi\pi}$ $[MeV/c^2]$	$\tilde{\Gamma}_{K\bar{K}}$ $[MeV/c^2]$
1	855	774	0
2	1268	1311	72
3	1493	14	116

Table 4.1: *K-matrix poles for $\pi\pi$ S-wave*

Since we don't know the $4\pi^0$ interaction at all, we use a free number of $J^{PC} = 0^{++}$ and $J^{PC} = 2^{++}$. Also we use several parameterisations for the background together with

the direct production of two ($\pi\pi$) S-waves plus a pion (constant in the F-vector). The decay of $4\pi^0$ resonances is described by two $\pi\pi$ S-waves. Up to now we don't take the possible decay of the $f_0 \to \pi(1300)\pi^0$ into account. That will be dine as soon as possible. The decay angular distribution is shown in tab. 4.2

J^{PC} of $4\pi^0$ resonance	angular distribution
0^{++}	1
2^{++}	$(cos^2\theta - \frac{1}{3})^2$

Table 4.2: *Angular distributions for the decay of the $4\pi^0$ resonances. θ is given in the rest frame of the resonance.*

When extending the isobar model to $4\pi^0$ resonances it is not clear, what phase space factors and center of mass momenta we have to use. When we think of the two $\pi\pi$ S-waves as of two particles, namely A and B, with the defined masses m_A and m_B, the phase space factor has a behaviour of a $m_A + m_B$-threshold. For every new combination of pions, we have new m_A and m_B and so new threshholds. A second effect of this choice is that the T-matrix pole position for the $4\pi^0$ resonance is not stable. To avoid this unphysical features we use the $4\pi^0$ threshold still taking two-body phasespace factors. Of course this description is not consistent but it tries to combine a clear threshold behaviour and the isobar model.

We start our fit procedure using a 0^{++} resonance with m=1373 and Γ=432 observed in the $\pi^+\pi\pi^0\pi^0\pi^0$ final state [7] by its $\sigma\sigma$ decay mode (fit 0). Using free mass and width just gives a small improvement of -17 in likelihood (fit 1). The best fits are obtained using a combination of a $f_0(1500)$ decaying into $4\pi^0$ together with a $\pi(1300)$ recoiling against a $\pi\pi$ S-wave and a some background contribution (fits 4,6 and 7). For mass and width of the $f_0(1500)$ we find 1500$\pm$10 MeV and 185 $\pm$ 20 MeV, respectively. The existence of a $pi(1300)$ and its contribution to the final state is not very well proofed because, due to its large width, it is not well distinguishable from the direct production of two $\pi\pi$ S-waves and a pion. But from fit #8 we see, that the $\pi(1300)$ cannot be substituted completely by a d_0 background.

We have tried two fits with different starting values for d_0, and indeed the fit finds two different local minima (fits 7 and 10). Also the different contributions vary. Since fit 10 is in much better agreement to the other good fits than fit 7, we trust more in fit 10. The constant background g contributes with 10-15%, which is in good agreement to the background estimated via Monte Carlo events.

To give a branching ratio for the $f_0(1500)$, decaying into $4\pi^0$ via two $\pi\pi$ S-waves, we fix the mass and width to the value found by the coupled channel analysis of Stefan Spanier to m=1505 MeV and Γ=154 MeV. Again the fit finds two different minima for hte background $d_0 + g$, but the contribution of the $f_0(1500)$ is stable with 30$\pm$3%. We generated 1438412 $5\pi^0$Monte Carlo events. The analysis chain found 1225000 events without tracks and ended with 164901 $5\pi^0$ events (already with a cut on the η-mass). This number then was corrected to an estimated background contribution of 14% (see Monte Carlo studies). We got 141815 correctly constructed $5\pi^0$For real data, we have 299259 $5\pi^0$ (after subtraction of η). The fit finds a constant background contribution of about

14%, what is in very good agreement to the estimated background. Subtracting this we find 257363 $5\pi^0$Ẇe calculate the branching ratio of $5\pi^0$ in all neutrals (without η) to

$$\frac{Br(\bar{p}p \to 5\pi^0)}{Br(\text{all neutrals}} = 16\%. \tag{4.9}$$

Assuming 4% all neutral events for all annihilations, a 30% fraction of the $f_0(1500)$,a branching ratio of $\pi^0 \to \gamma\gamma = 0.988$ and a factor of 9 due to isospin, we get, taking also charged pions into accout:

$$\frac{Br(\bar{p}p \to f_0(1500) \to 4\pi}{Br(\text{all}} = 1.8 \cdot 10^{-2}. \tag{4.10}$$

Fit #	$\pi(1300)$		0^{++}		2^{++}		backgr.	$-ln\mathcal{L}$
	m	Γ	m	Γ	m	Γ		
0	–	–	1373(fix)	432(fix)	–	–	–	470145
1	–	–	1373	404	–	–	–	-17
2	1268	391	–	–	–	–	–	+1115
3	–	–	851	2587	–	–	–	-734
			1718	844	–	–	–	
4	1075	352	1496	172	1275 (fix)	185 (fix)	g	-1131
5	–	–	1381	376	769	1546	–	-277
6	1075	344	1495	171	–	–	g	-1112
7	1107	306	1507	208	–	–	$d_0 + g$	-1180
8	–	–	14887	242	–	–	$d_0 + g$	-785
9	–	–	– –	–	–	$d_0 + g$	+4301	
10	1066	375	1500	181	–	–	$d_0 + g$	-1140
11	1078	349	1505(fix)	154(fix)	–	–	g	-1086
12	1092	344	1505(fix)	154(fix)	–	–	$d_0 + g$	-1105
13	1106	257	1505(fix)	154(fix)	–	–	$d_0 + g$	-1107

Table 4.3: *Fit results for $5\pi^0$ partial wave analysis. All masses and widths are in MeV/c^2. Background: g: constant background, d_0: constant added to F-vector in 0^{++}-channel, d_2: constant added to F-vector in 2^{++}-channel*

Fit #	$\pi(1300)$	0^{++}	2^{++}	backgr.
0	–	100%	–	–
1	–	100%	–	–
2	100%	–	–	–
3	–	86%	–	–
		14%	–	–
4	55.5%	32.4%	0.1%	12%
5	–	98.5%	1,5%	–
6	54.5%	33.5%	–	12%
7	18%	50%	–	17+15%
8	–	51%	–	31+15%
9	–	–	–	100+0%
10	58%	26%	–	1+15%
11	60%	28%	–	12%
12	55%	33%	–	1+11%
13	50%	28%	–	14+8%

Table 4.4: *Contributions to final state.*

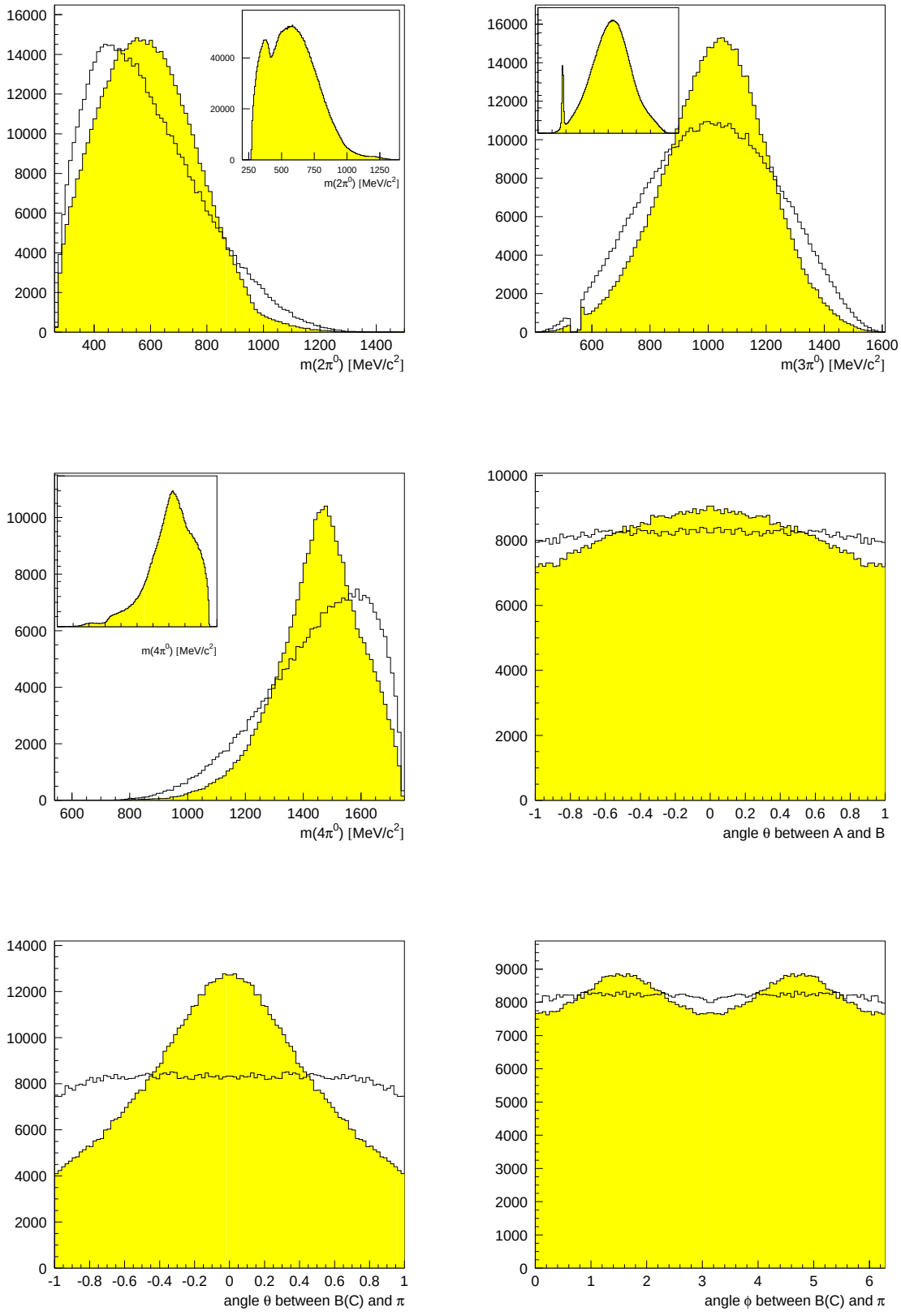

Figure 4.2: *Invariant mass and decay angular distributions of the $5\pi^0$ final state. Small pictures: data befor η reduction. Grey distributions show data.*

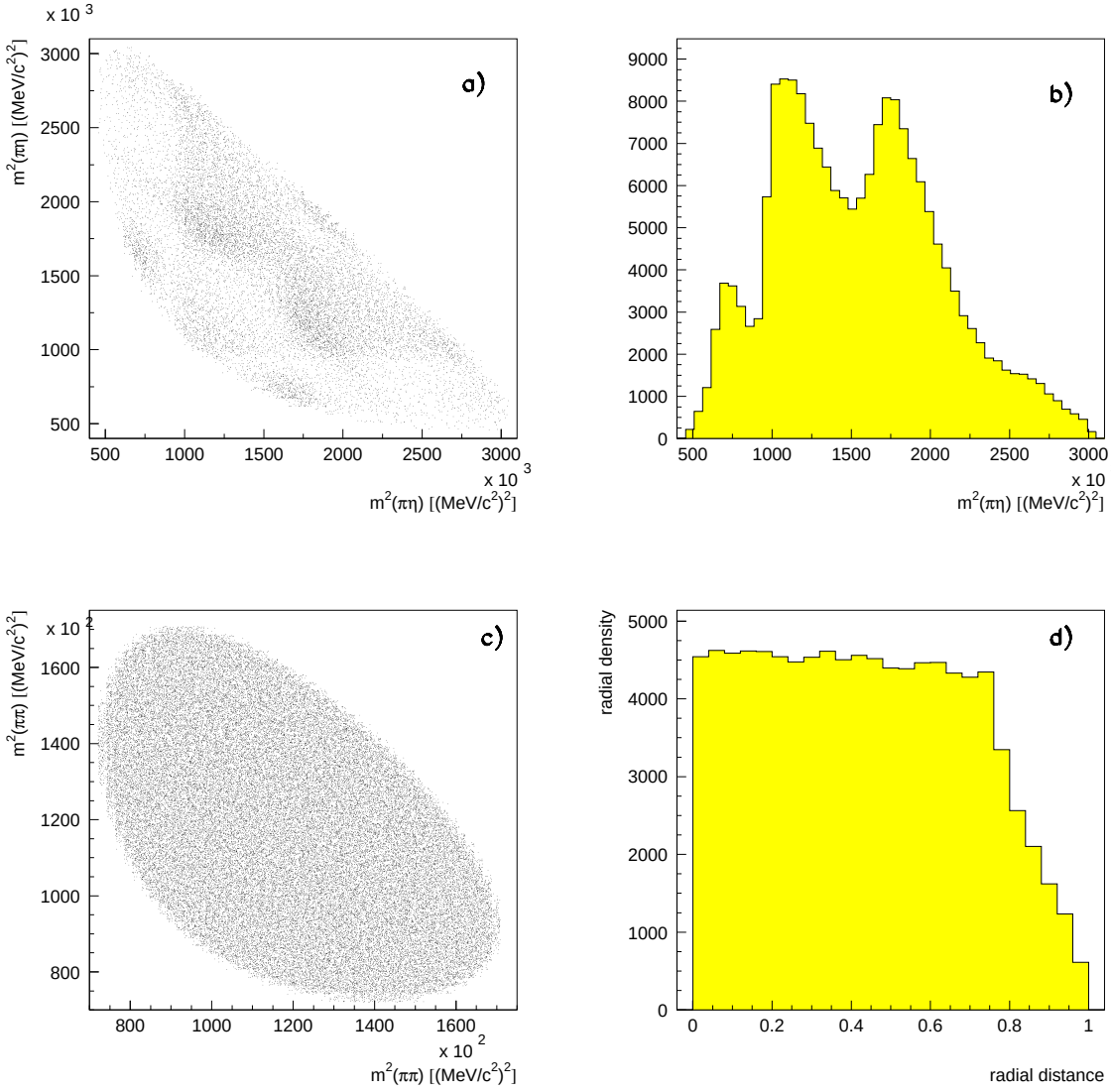

Figure 4.3: *The $\pi\pi\eta$ final state.*

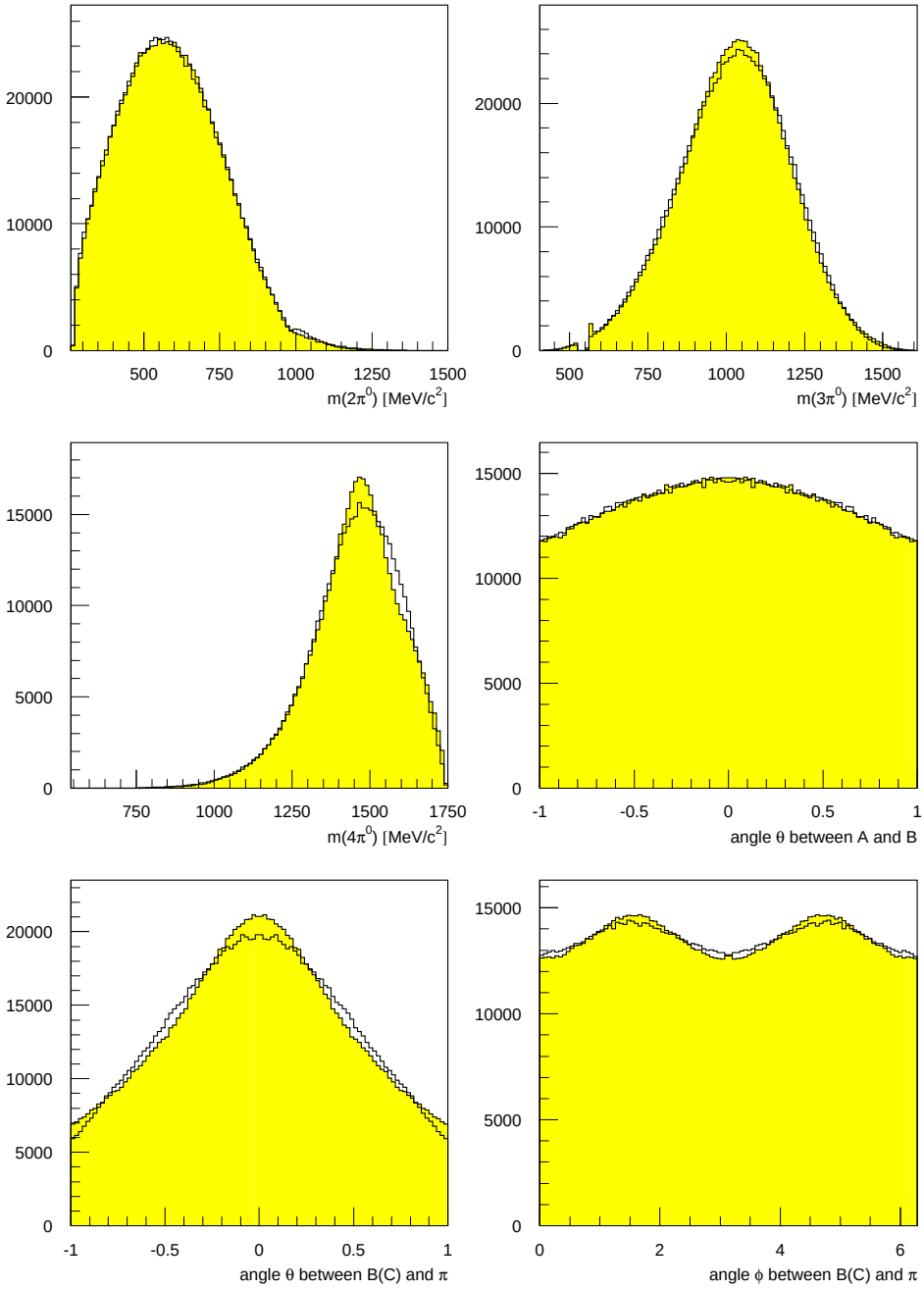

Figure 4.4: Mass and angular distributions. Fit 0 compared to data.

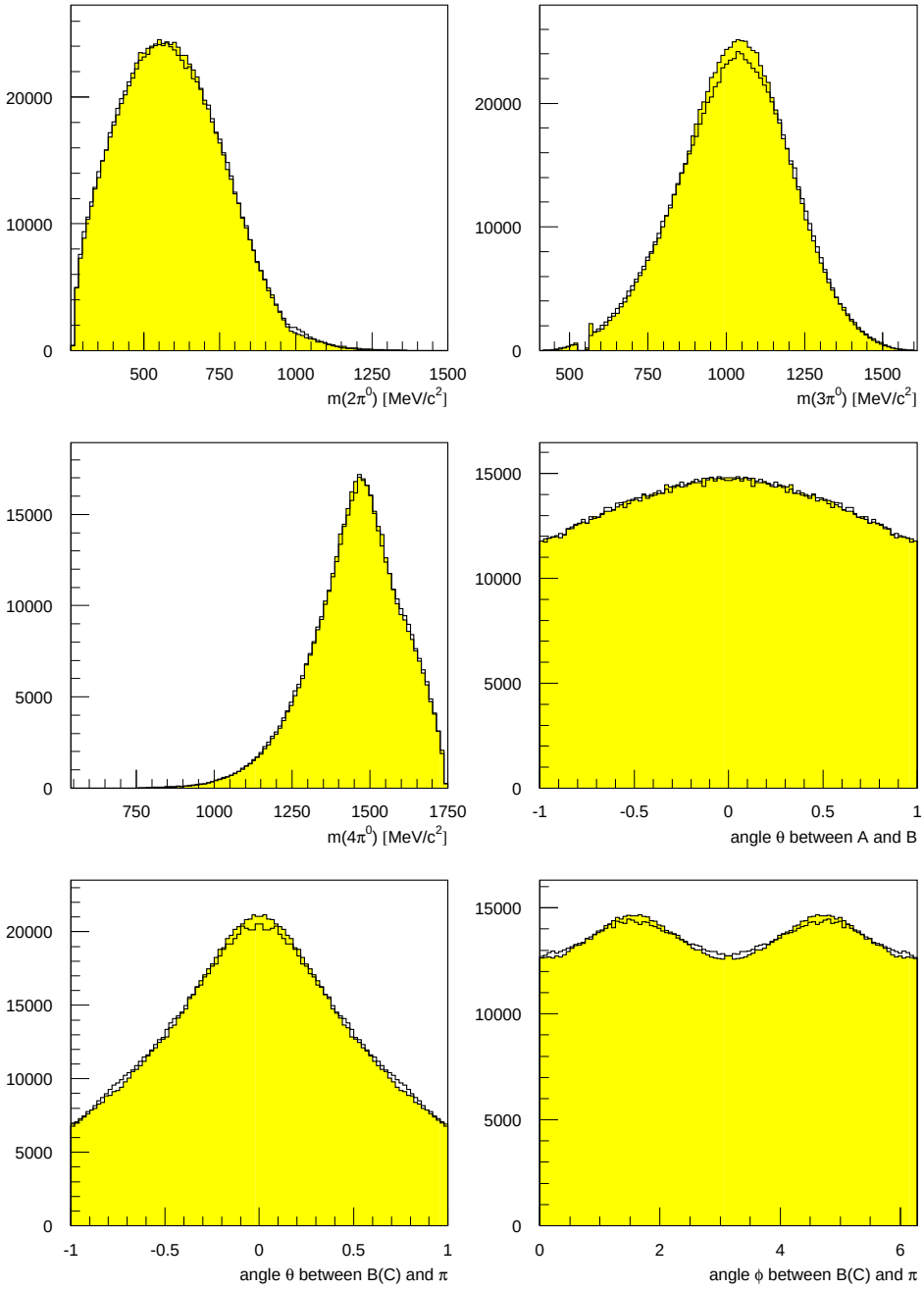

Figure 4.5: Mass and angular distributions. Fit 6 compared to data.

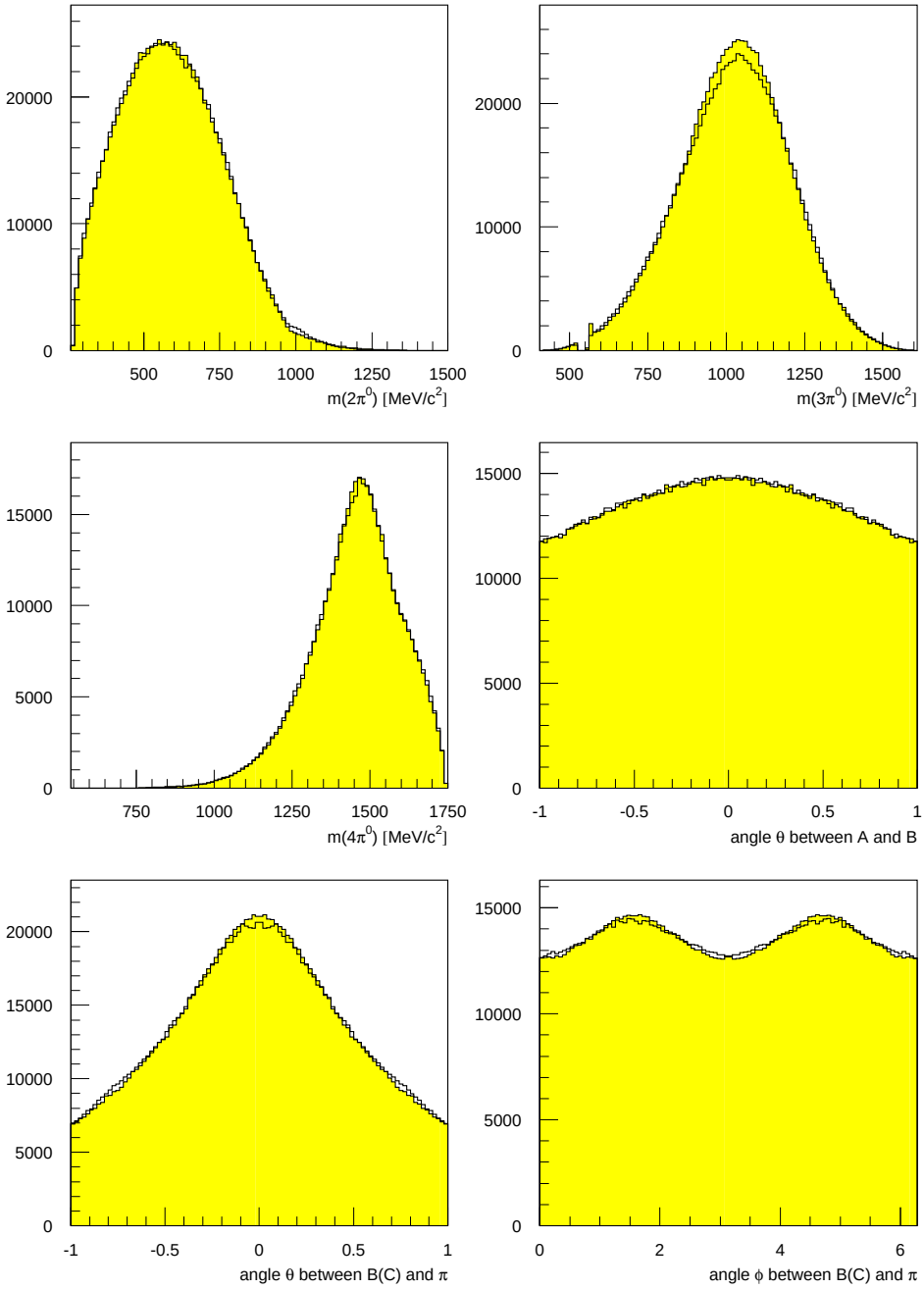

Figure 4.6: Mass and angular distributions. Fit 7 compared to data.

Bibliography

[1] Ralf Hackmann, Technical report $\pi^0\eta\eta$ analysis, CB-note 273 Universität Bonn, 1994.

[2] C. Amsler et al., High statistics study of the $f_0(1500)$ decay into $\eta\eta$ submitted to Phys. Lett. **B**(1995).

[3] C. Amsler et al., (Crystal Barrel Collaboration Phys. Lett. **B333**(1995)277-282.

[4] Review of Particle Properties: L. Montanet et al. Phys. Rev. **D50** (1994)1198.

[5] S. U. Chung et al., Partial wave analysis in K-matrix formalism Mainz report.

[6] J. Brose, Beobachtung einer neuen $J^{PC} = 0^{++}$-Resonanz in der Antiproton-Proton-Vernichtung in $\pi^0\pi^0\pi^0$. Dissertation, Mainz 1994.

[7] C. Amsler et al., (Crystal Barrel Collaboration) Phys. Lett. **B322** (1994)431.